Chipless RFID Sensor Tag for Metal Crack Detection and Characterization

Adi Mahmud Jaya Marindra and Gui Yun Tian, *Senior Member, IEEE*

***Abstract*—Chipped radio frequency identification (RFID) sensor systems have been studied for structural health monitoring (SHM) applications. However, the use of chipped sensor tags and its standardized narrowband operation contribute shortcomings in cost, durability, and detection capability. This paper presents a novel use of the frequency signature based chipless RFID for metal crack detection and characterization operating in ultra-wideband (UWB) frequency. The vision is to implement a low-cost and high-temperature-resistant passive wireless sensor able to monitor the crack on a metallic structure with multi-parameter detection. We propose a chipless RFID sensor tag integrating four tip-loaded dipole resonators as a 4-bit ID encoder and a circular microstrip patch antenna (CMPA) resonator as a crack sensor. The radar cross section (RCS) spectrum of the chipless RFID sensor tag generates four resonant frequencies from the dipole resonators and a resonant frequency from the CMPA resonator. Simulation and experimental results show that the resonant frequency shift of the CMPA is a useful feature to indicate the crack orientation and the crack width on a metallic structure. The direction of the resonant frequency shift represents the orientation of crack, while the magnitude of the resonant frequency shift is proportional to the width of the crack. Furthermore, the experimentation with a natural fatigue crack sample proves that the proposed sensor tag is capable to detect submillimeter cracks.**

***Index Terms*— chipless RFID, microstrip patch antenna, structural health monitoring (SHM), wireless crack sensor**

I. Introduction

STRUCTURAL health monitoring (SHM) is the integration of sensor technologies and the internet of things (IoT) to implement automatic detection systems of structural damages on mechanical and civil infrastructures [1, 2]. The acquired information from IoT-based SHM systems can benefit us in life-cycle assessments, asset managements, and preventing failures on invaluable infrastructures such as bridges, wind turbines, aircrafts, and pipelines [3]. Without SHM systems, unmonitored cracks due to fatigue or corrosion on metallic structures may cause hazardous incidents and therefore jeopardize human safety. This is of the uttermost importance to monitor the health condition of safety-critical infrastructures, in order to prevent catastrophic failures, also to reduce manual maintenance costs. A widely-known solution for metal inspection is to utilize non-destructive testing and evaluation (NDT&E) techniques, e.g. liquid penetrant testing [4], ultrasonic testing [5], eddy current testing [6], thermography testing [7], and microwave waveguide testing [8], which have shown good detection sensitivity and reliability. However, these close-range inspection approaches are time consuming, cost much in labors, and practically too cumbersome for SHM applications [9].

To bridge the gap between NDT&E and SHM, radio frequency identification (RFID)-based sensor systems are attractive because RFID is wireless, passive, and low-cost [10, 11]. Previous studies have investigated the use of RFID tag antennas as sensors, especially the ultra-high frequency (UHF) RFID, for metal crack detection and characterization [12-14]. It was reported that, by using phase shift feature from a coupled dipole RFID tags, a submillimeter crack can be detected from 1.5 m distance [12]. Longer reading range, roughly 2.1 m, is achieved with a folded rectangular patch antenna, but the size of the sensor tag is too big [13]. For miniaturization purpose, a 3-by-3 cm size 3D folded dipole RFID tag, reportedly, can detect a crack from 1 m distance using the backscattered power feature in conjunction with principal component analysis (PCA) to reduce the environmental effects [14]. Although the studies have proved the feasibility, however, the use of application specific integrated circuit (ASIC) makes chipped RFID sensor tags not cost-effective and unable to work in harsh environments such as in high temperature condition. Furthermore, the detection capability of chipped RFID sensor systems is limited to only one parameter detection, i.e. the crack width, due to the fact that chipped RFID standards operate within a narrowband spectrum.

Chipless RFID, the next generation of RFID, offers several advantages over the chipped RFID in terms of cost, simplicity, printability, and ability to work in high temperature environments [15-17]. Therefore, chipless RFID recently has drawn great attentions in sensor applications [18, 19]. One notable progress is the multi-parameter frequency signature based chipless RFID sensor having a capability of detecting multiple physical variables [20]. The idea of using chipless technologies for crack detection is relatively new. Previously,

Manuscript received; revised; accepted. Date of publication. This paragraph of the first footnote will contain the date on which you submitted your paper for review. This work was supported in part by the Engineering and Physical Sciences Research Council (EPSRC). The work of A. M. J. Marindra was supported by the Indonesia Endowment Fund for Education (LPDP) within the Ministry of Finance, Indonesia.

The authors are with the School of Electrical, Electronic, and Computer Engineering, Newcastle University, Newcastle upon Tyne NE1 7RU, UK (e-mail: a.m.j.marindra2@newcastle.ac.uk; g.y.tian@ncl.ac.uk).

Color versions of one or more of the figures in this paper are available online at

Digital Object Identifier

the time domain reflectometry (TDR)-based chipless RFID with delay-line tag structure [21], the frequency selective surface (FSS) based sensor [22], and the harmonic tag using band-stop filter structure [23] have been observed for detecting crack on non-metallic structures. In principle, the crack on the non-metallic object will break the sensor and change the sensor's electromagnetic characteristics. Patch antenna is chipless and has been studied for metal crack detection, but unlike the RFID sensor systems, antenna sensors need to be read by wire from the antenna terminal [24]. Nonetheless, as per authors' knowledge, utilization of the frequency signature based chipless RFID for metal crack detection has not been investigated.

This study reports a novel use of the frequency signature based chipless RFID sensor tag for metal crack detection and characterization. The proposed sensor tag operates in UWB frequency, integrating dipole resonators as ID encoders and a circular microstrip patch antenna (CMPA) resonator as a crack sensor. By using the resonant frequency shift of the CMPA, the proposed sensor can detect and characterize two crack parameters, i.e. crack orientation and crack width. This multi-parameter detection capability has never been achieved by chipped RFID sensors. Crack width is a crucial parameter to signify the severity of a crack, while crack orientation is useful for knowing the crack progression. The direction of resonant frequency shift represents the crack orientation, while its magnitude is proportional to the crack width. With this multi-parameter detection capability, we have shown a remarkable potential of chipless RFID sensor system for metal crack detection and characterization.

II. Crack Detection Approach

The working principle of chipless RFID sensor system for crack detection and characterization can be seen in Fig. 1. The sensor reader interrogates the sensor tag mounted on a metallic structure by transmitting a broadband signal through the Tx antenna. Reflection from the sensor tag and the metal results in backscattered signal, which will be received by the Rx antenna. Next, the sensor reader performs signal processing and feature extraction to identify the tag ID as well as to read the sensor information. In this system, the sensor tag is an important part to shape the backscattered signal, forming signature in frequency domain and unique sensing features, for telling the reader if any crack presented on the metallic structure.

Since the concern of this study is crack detection on metallic structures, a design requirement to meet is that the sensor tag must be 'metal-mountable'. A metal-mountable sensor tag design needs to consider metal as an integral part of the tag. By this consideration, two-layer chipless RFID tag designs backed with a ground plane can operate well on metal. The reason is that the metallic surface, on which the tag is mounted, acts similarly as the tag's ground plane [25, 26]. The following designs are some reported chipless RFID tag structures with ground plane: dipole [27], folded dipole [28], stepped impedance resonator [29], closed-loop resonator [30, 31], and microstrip patch [32]. Among the feasible metal-mountable designs, this study takes an interest in circular microstrip patch antenna (CMPA) seeing that a study has revealed its good performance for omnidirectional strain detection [33]. The CMPA sensor has shown a clear difference when the strain is applied with 0˚ orientation and 90˚ orientation. The resonant frequency will shift towards lower frequencies for 0˚-oriented strain, and oppositely, it will shift towards higher frequencies for 90˚-oriented strain. This evidence is a motivation to assume that a circular shape with its geometric uniformity would also have good results for detecting different crack orientations.

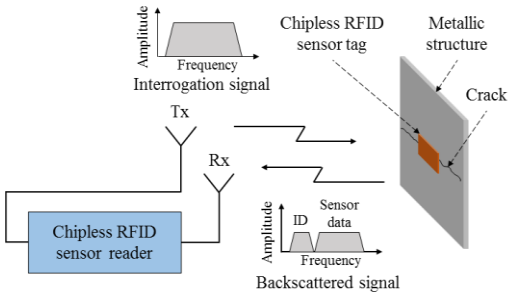

Fig. 1. Principle of chipless RFID sensor system for crack detection and characterization on a metallic structure

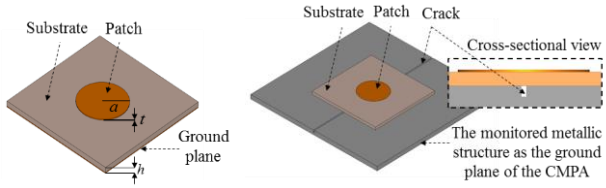

(a) (b)

Fig. 2. Circular microstrip patch antenna (CMPA) structure: (a) The typical configuration, (b) The modified configuration when the antenna applied for crack sensor on a metallic structure

A typical structure of CMPA is shown in Fig. 2(a). In theory, the supported modes and resonant frequency of a CMPA are found by treating the patch, the ground plane and the material between them as a circular cavity [34]. It is noteworthy that the fundamental resonant frequency of CMPA will not change significantly with external wireless excitation [35]. When a CMPA is applied for a metal crack sensor, only a circular patch is printed on the top layer of substrate while the surface of the monitored metallic structure is considered as the ground plane as illustrated in Fig. 2(b). Consequently, the electrical properties and the physical condition of the metal underneath of the patch, such as a presence of crack, affect characteristics of the CMPA. A metal crack can be defined as an open line on a metallic surface along which it has split yet without breaking apart the structure. The presence of crack in the ground plane will modify the formed circular cavity of CMPA because the crack emerges an open gap filled by air in the ground plane. This change will affect the antenna mode and also the antenna effective radius considering that the substrate thickness and the permittivity needs to take into account of the presented air gap due to the crack. Since the resonant frequency is dependent to the antenna effective radius, the presence of crack can be detected by using the resonant frequency shift of the CMPA.

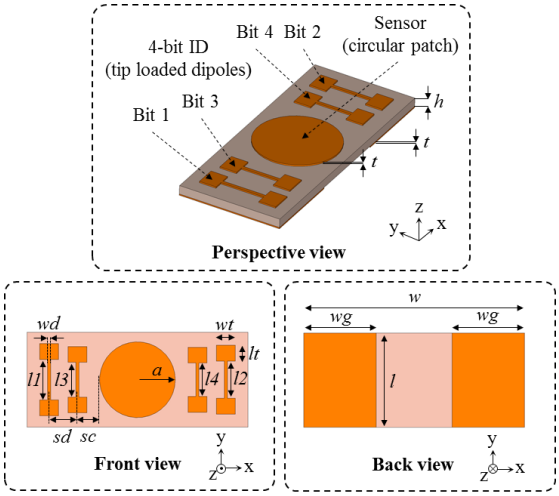

Fig. 3. Layout of the proposed chipless RFID sensor tag

TABLE I
DIMENSION OF THE PROPOSED CHIPLESS RFID SENSOR TAG (IN MM)

a	*h*	*l*	*l1*	*l2*	*l3*	*l4*	*lt*	*sc*	*sd*	*t*	*w*	*wd*	*wg*	*wt*
6	1.27	15	6.4	5.9	5.5	5.3	2.5	3.5	4.5	0.035	35	0.5	11.5	3

III. CHIPLESS RFID SENSOR TAG DESIGN

Layout and dimension of the proposed chipless RFID sensor tag is presented in Fig. 3 and Table 1, respectively. The sensor tag is designed on a Taconic CER-10-0500 laminate with the dielectric constant (ε_r) of 10 and the loss tangent (δ) of 0.0035. A substrate with a high dielectric constant is chosen in order to minimize the size of the sensor tag and maximize the quality factor (Q). The overall size of the chipless RFID sensor tag is 35 mm x 15 mm. The proposed sensor tag consists of two parts of resonators: sensor part and ID part. The sensor part of the tag is a CMPA resonator as described in the previous section, while the ID part consists of four tip-loaded dipole resonators positioned on the left and right sides of the circular patch. These four ID resonators are to generate a binary ID of '1111'. On the sensor tag's backside (see the tag's back view in Fig. 3), the ground plane is created only at the backside of ID resonators because the ground plane for circular patch is the monitored metallic structure. The inherent ground plane on the backside of ID resonators is to protect the ID signature so that the ID of the tag will not be affected by the presence of crack on the metallic structure.

Dipole shape is chosen for ID resonators because of its simple geometry and its ability to resonate on a ground plane. A dipole on a ground plane works as a half wavelength resonator that will have a resonant frequency depending on its length. In our proposed design, the dipole shape is modified with the capacitive tip loading structure, by enlarging both dipole's tips, beneficial to shorten the dipole physical length and to reduce mutual coupling between the resonators. The tip-loaded structure reduces the mutual coupling by making the surface current distributed on the ground plane to be more concentrated, and thus less interfering the adjacent resonators. The real impact of this mutual coupling reduction is that the resonators can be placed closer to each other so that the overall size of the sensor tag decreases significantly over the use of normal dipoles. It is worth to note that despite of the tag's structure and dimensions, spacing between resonators and their placement order need to be designed carefully due to the mutual coupling issue. First, the spacing between resonators needs to be reasonably large. Second, two dipole resonators with slightly different lengths should not be placed closely as they produce adjacent resonant frequencies. This is the reason why in our design, two ID resonators are placed on the left side of the circular patch and the other two are placed on the right side. Since multiple resonators are placed on the same surface like an array, there are electromagnetic interactions where the current developed in each resonator also depends on the contributions from the adjacent resonators. Reducing mutual coupling among the resonators with the mentioned techniques will ensure that each resonator produce resonant frequency distinctly.

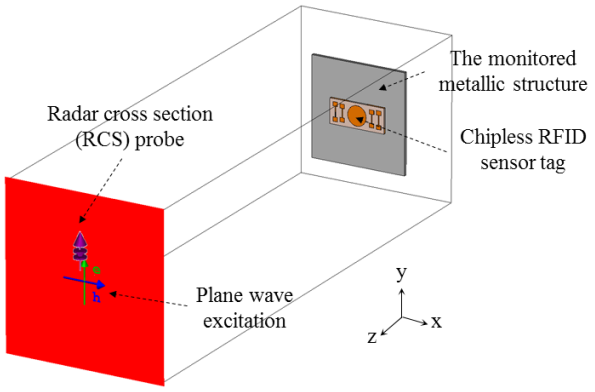

Fig. 4. Simulation setup of the chipless RFID sensor tag

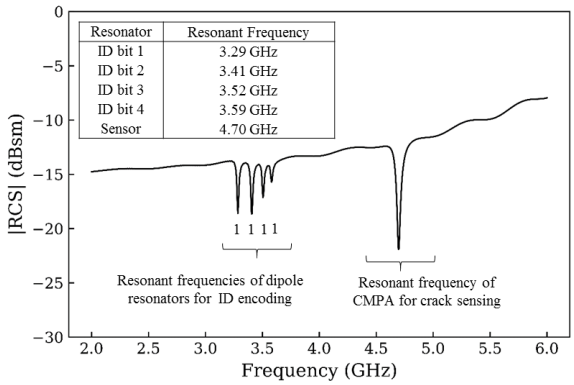

Fig. 5. Simulated RCS spectrum of the chipless RFID sensor tag showing two sets of resonant frequency

The chipless RFID sensor tag is designed and simulated in CST Microwave Studio® with a simulation setup depicted in Fig. 4. The sensor tag is placed on a metallic plate with a dimension of 60 mm x 60 mm x 2 mm and an electrical conductivity (σ) of 3.56 x 10^7 S/m. Acting as the chipless RFID reader, a plane wave excitation and a radar cross section (RCS) probe are set in the model positioned at 30 cm in front of the sensor tag. The plane wave excitation transmits linearly polarized signal to –z direction with its E-plane parallel to the

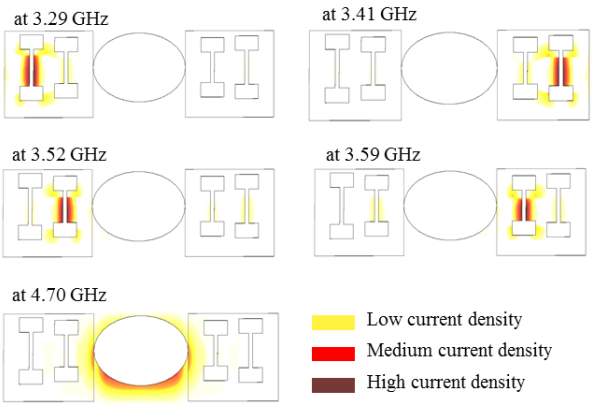

Fig. 6. Surface current distributions of the chipless RFID sensor tag showing the concentration of current at each resonant frequency

y-axis and its H-plane parallel to the x-axis. The RCS probe acquires RCS spectrum, which is a measure of ratio of the backscattered signal power to the power density that is intercepted by the sensor tag and the metallic structure. The RCS spectrum contains resonant frequencies produced the by resonating structures on the sensor tag.

The setup is simulated within a frequency range of 2 GHz to 6 GHz by using an 'open (add space)' boundary setting for all axis directions. Fig. 5 shows the simulated RCS spectrum of the chipless RFID sensor tag. When a plane wave excites the sensor tag, it shows a frequency selective behavior with deep notches at the resonant frequencies of the resonators. The notches are formed because the conductive structures in the tag resonate the excitation signal at certain frequencies causing some energy at those frequencies to be absorbed before it is reflected. It is obvious that the sensor tag produces two sets of resonant frequency within the UWB frequency (3.1-10.6 GHz). The first set of resonant frequency is the ID signature that consists of four resonant frequencies at 3.29 GHz, 3.41 GHz, 3.52 GHz, and 3.59 GHz. The second set of resonant frequency is a sensor data signature produced by the CMPA at 4.70 GHz. The ID signature encodes a tag ID of '1111' since four resonant frequency notches are present. The tag ID can be modified by either eliminating the corresponding ID resonator/s or equalizing its length to a resonator which has ID bit of '1'. For example, a tag ID of '1011' can be obtained by eliminating the resonator of bit 2 or equalizing its length to the resonator of bit 1. Changing the ID bit state from '1' to '0' is essentially done by making the resonant peak absent in the ID data signature.

To relate the resulting resonant frequencies with the tag structure physically, the surface current distributions of the sensor tag at different frequencies are presented in Fig 6. It can be seen that each resonator manifests a strong surface current at a particular resonant frequency. At the frequencies of 3.29 GHz, 3.41 GHz, 3.52 GHz, 3.59 GHz, 4.70 GHz, the strongest current appears at the location of dipole resonator of bit 1, bit 2, bit 3, bit 4, and CMPA, respectively. Thus, it is confirmed that the resonant frequencies are contributions from each individual resonator. It is also important to notice that the

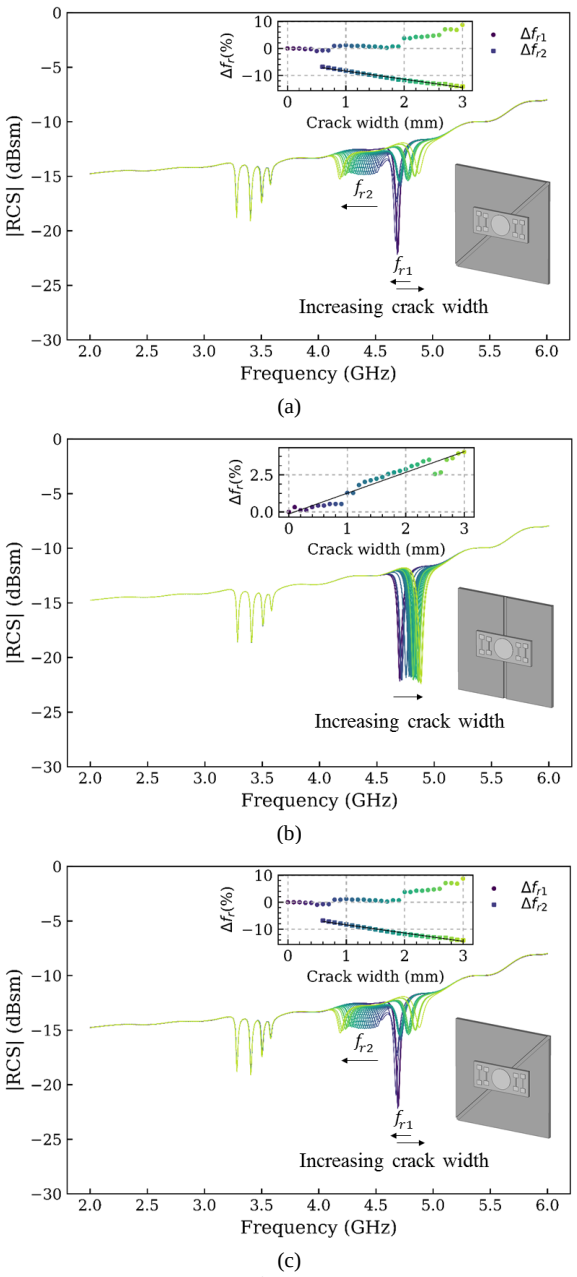

Fig. 7. Simulated RCS spectra of the chipless RFID sensor tag showing resonant frequency shift for different crack orientations and widths: (a) Horizontal crack, (b) Vertical crack, (c) Diagonal crack

strong current is more distributed on the ground plane's surface rather than on the resonator's surface. Hence, any change on RCS spectrum, in respect to physical change on the metallic structure, can be analyzed based on the surface current distribution.

IV. Simulation Study On Metal Crack Detection And Characterization

To study the effect of crack, a crack is constructed artificially along the monitored metallic structure and the RCS spectrum is simulated for different crack orientations and crack widths. Since the sensor tag is placed at the center of the metallic surface, the constructed crack will pass through the

backside of the circular patch. We investigate different widths of metal crack with 0˚ orientation (horizontal crack), 90˚ orientation (vertical crack), and 45˚ orientation (diagonal crack). Horizontal cracks are defined as the cracks whose orientation is perpendicular to the E-plane while vertical cracks are defined as the cracks whose orientation is parallel to the E-plane. For each crack orientation, we perform parametric sweep in which the crack depth is fixed at 1 mm whilst the crack width is varied from 0 mm to 3 mm by 0.1 mm step.

In metal crack detection, only the sensor's resonant frequency is expected to change according to the orientation and the width of the crack. The simulated RCS spectra of the chipless RFID sensor tag for different crack orientations and widths are presented in Fig. 7. It is apparent that a crack will shift the sensor data signature without affecting the ID signature. In general, a crack will shift the resonant frequency of the CMPA with different directions and magnitudes depending on the orientation and the width of the crack. We use the direction and the magnitude of resonant frequency shift as features to characterize the crack orientation and the crack width, respectively. The normalized magnitude of resonant frequency shift (Δf_r) in percentage can be represented as

$$\Delta f_r(\%) = \frac{f_r^{new} - f_r^{initial}}{f_r^{initial}} \times 100 \quad (1)$$

where $f_r^{initial}$ is the resonant frequency of the CMPA without the presence of crack and f_r^{new} is the resonant frequency of the CMPA after the crack occurred. The numerical sign $\Delta f_r(\%)$ can shows whether the resonant frequency of CMPA shifts toward a lower frequency or a higher frequency.

Fig. 7(a) shows that a horizontal crack will linearly shift the resonant frequency to lower frequencies as the crack width increased. The detection sensitivity can be calculated by taking an average change of resonant frequency per a certain unit of crack width. For horizontal crack, the detection sensitivity is approximately $\Delta f_r(\%) = -0.28\%$ or –13.43 MHz shift per 0.1 mm increase of the crack width. In opposite to the horizontal crack, a vertical crack shifts the resonant frequency towards higher frequencies as can be seen in Fig. 7(b). In general, the trend of resonant frequency shift for vertical crack detection is linear. The detection sensitivity in vertical crack detection is averagely $\Delta f_r(\%) = +0.14\%$ or +6.67 MHz shift per 0.1 mm increase of the crack width. Indeed, the resonant frequency shift is seen to be not linear at some crack widths. Nonetheless, we can still justify whether a vertical crack is present as long as the resonant frequency is shifted to a higher frequency. The constraint is that, at some degree, the resonant frequency does not represent width of the vertical crack accurately.

A diagonal crack detection is somewhat more difficult because it relies on two resonant frequencies as shown in Fig. 7(c). Here, the shifts from those two resonant frequencies are named as Δf_{r1} and Δf_{r2}. Up to 0.5 mm width, the presence of a diagonal crack can be detected by recognizing the slight shift from Δf_{r1}. However, the crack orientation and the crack width cannot be characterized since the trend of Δf_{r1} is irregular. Higher than 0.6 mm width, the Δf_{r2} can be identified and it decreases proportionally as the crack width increased. The Δf_{r2} decreases –0.31% or –15.3 MHz per 0.1 mm increase of crack width. Hence, a diagonal crack can be detected when two resonant frequencies are present. The Δf_{r2} can be used as a feature to characterize the crack width. A limitation in the diagonal crack detection is that when the width is too small, i.e. less than 0.6 mm, the crack can be misinterpreted as if it does not exist or might detected as a horizontal crack.

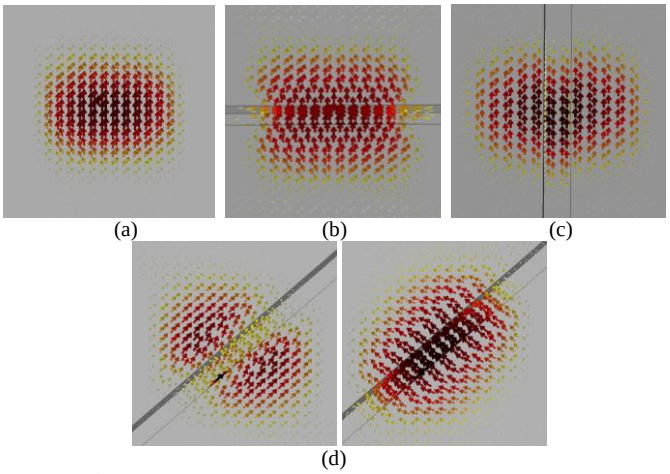

Fig. 8. Surface current distribution on the metallic structure under the CMPA showing the current flows for different crack orientations: (a) Without crack: at 4.70 GHz, (b) With a 2-mm horizontal crack: at 4.43 GHz, (c) With a 2-mm vertical crack: at 4.84 GHz, (d) With a 2-mm diagonal crack: at 4.30 GHz (left) and 4.77 GHz (right)

To understand how the crack shifts the resonant frequency in different ways, we observe the surface current distribution for different crack orientations as provided in Fig. 8. As can be seen in Fig. 8(a), most current paths flowing on a normal metallic structure are in parallel direction with E-plane at the resonant frequency. Meanwhile, the outer side current paths are curved following the shape of the CMPA, which is circular. When a horizontal crack is present in the ground plane as in Fig. 8(b), it will force the current to flow across the crack cavity. The horizontal crack will lengthen the current paths and essentially increases the electrical length of the CMPA. The wider the horizontal crack, the electrical length of the CMPA will be longer. Since the resonant frequency is inversely proportional to electrical length of an antenna, a horizontal crack will shift the resonant frequency of CMPA to lower frequencies. In Fig. 8(c), it is shown that a vertical crack will displace some current paths to the crack bottom surface. This portion of current, which flows on the crack bottom, will not be taken into account of determining the CMPA effective radius. Thus, due to the current displacement, a vertical crack decreases the electrical length of the CMPA by means of decreasing its effective radius and consequently shifts the resonant frequency to higher frequencies. A diagonal crack

Fig. 9. Fabricated chipless RFID sensor tag

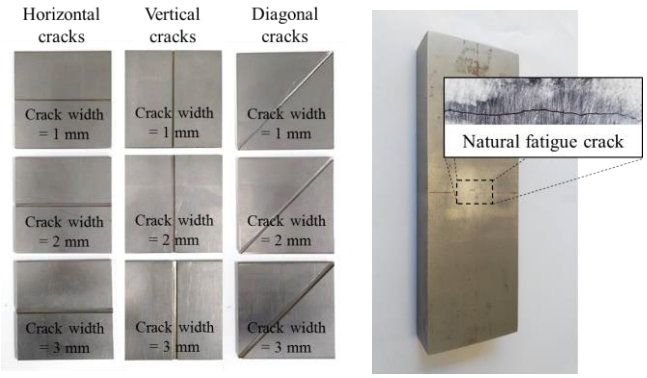

Fig. 10. Metal crack samples: (a) Artificial crack samples, (b) Natural fatigue crack sample

combines both phenomena. When a sizeable diagonal crack is present, the CMPA operates in two resonant modes as displayed in Fig. 8(d). The first mode is when the current splits and flows diagonally alongside the crack while there is a small amount of current flows across the crack. In this mode, the trend of the resulting resonant frequencies from different widths of crack is somehow irregular because the electrical length of the CMPA now depends on not only the length of the diagonal current paths, but also the amount of current that can flow across the crack. Another mode is created when the current flows diagonally across the crack so that the length of current paths increases as the crack widened. This mode is similar to the phenomenon in horizontal crack detection which will induce a resonant frequency proportional to the width of crack.

V. Experimental Validation and Discussion

After investigating the performance of crack detection using simulation, the chipless RFID sensor tag is fabricated and validated through experimental studies. Fig. 9 depicts the fabricated chipless RFID sensor tag with a coin as size comparison. We also prepared nine artificial crack samples and a natural fatigue crack sample, as exhibited in Fig. 10, for the experiment. The artificial crack samples, shown in Fig. 10(a), are made from aluminum plates with three different crack orientations (horizontal, vertical, and diagonal) and three different crack widths (1 mm, 2 mm, and 3 mm). The natural fatigue crack sample, shown in Fig. 10(b), is on a steel bar having dimensions of 170 mm x 50 mm x 20 mm with a microscopic crack at the center of the bar's surface.

Fig. 11 illustrates the experiment setup using bistatic radar configuration. As depicted in Fig. 11(a), we used an Agilent 8363B vector network analyzer (VNA) connected to two identical standard gain horn antennas that can operate within the range of 1 GHz to 18 GHz band. Two horn antennas are separated by a distance of 5 cm. Although the reader antennas

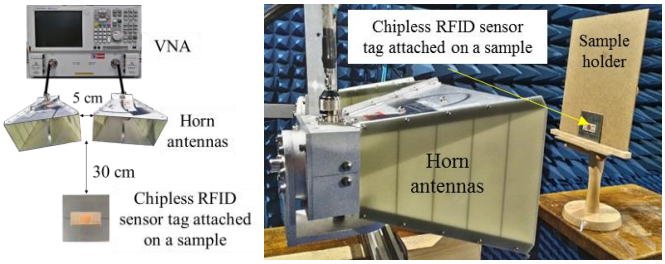

Fig. 11. Experiment setup using bistatic radar configuration: (a) Diagram of the experimental setup, (b) Photograph showing the positioning of horn antennas and the sensor tag inside an anechoic chamber

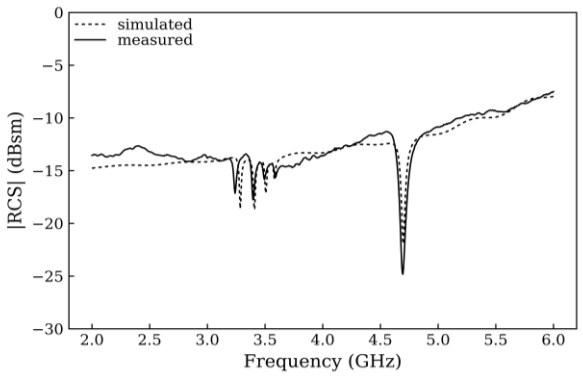

Fig. 12. Comparison between the simulated and the measured RCS spectra of the chipless RFID sensor tag

are placed side by side as in the monostatic radar configuration, this tag reading mechanism is considered as bistatic since the phase centers of the horn antennas are comparable to the distance between the horn antennas and the sensor tag. The chipless RFID sensor tag is attached on a metal crack sample by using an adhesive thin transparent tape. The tag and the metal sample are put upright in the sample holder towards the horn antennas and all positioned 30 cm in front of the horn antennas. After the two-port network standard calibration in the 2-6 GHz band is performed, Port 1 and Port 2 of the VNA are connected to horn antennas. The power delivered by the VNA is set as 0 dBm in the entire frequency band with an averaging function activated for 100 measurements to increase the signal to noise ratio.

To obtain RCS from measurement, we need to perform subtractions with the measurement background and scale the subtracted result using a reference RCS. First, the measured S_{21} of tag and sample ($S_{21}^{\text{tag+sample}}$) needs to be subtracted with an empty background measurement ($S_{21}^{\text{background}}$). The sample holder should be included in the empty background measurement as we need to obtain the RCS of tag and sample only. Second, we need to measure S_{21} of a reference object (S_{21}^{ref}) having a known RCS from simulation (RCS_{ref}) and to subtract it with the measured empty background. A 50 mm x 50 mm x 2 mm aluminum plate can be used as the reference object. Hence, the measured RCS can be obtained as [36]

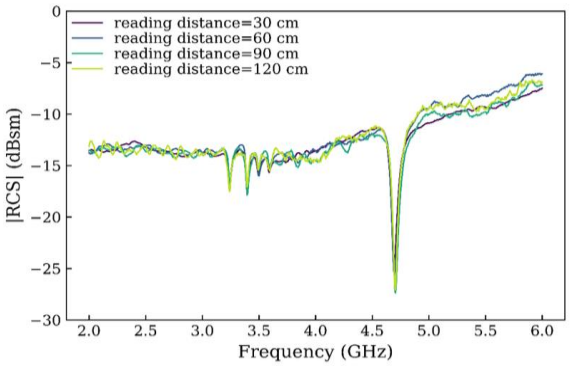

Fig. 13. Measured RCS spectra with different reading distances

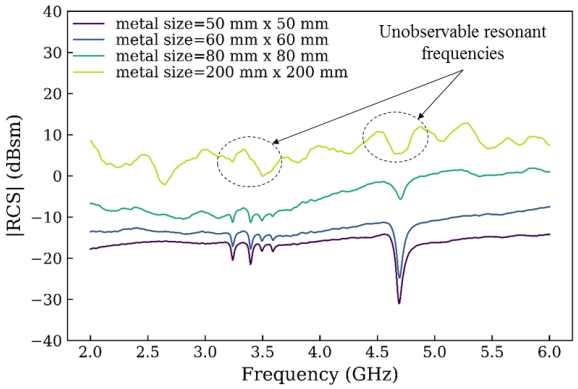

Fig. 14. Measured RCS spectra using (2) of the chipless RFID sensor tag placed on different sizes of metal sample showing unreadable tag if the metal size is 200 mm x 200 mm

$$\mathrm{RCS}_{\mathrm{tag+sample}} = \left[\frac{S_{21}^{\mathrm{tag+sample}} - S_{21}^{\mathrm{background}}}{S_{21}^{\mathrm{ref}} - S_{21}^{\mathrm{background}}}\right]^2 \cdot \mathrm{RCS}_{\mathrm{ref}} \quad (2)$$

Here, the metal sample has a dominant contribution in forming the RCS. When the size of metal sample is large as compared to the tag, the signal absorption can be too less compared to reflection leading to undetectable resonant frequencies. Hence, the original RCS written in (2) is dependent of the size of metal sample. Fortunately, we can isolate the RCS result from the reflection manifested by the metal sample, and leaving the absorption characteristic of the chipless RFID sensor tag. An inversion of RCS can show the ability of the chipless RFID sensor tag to absorb signals in the direction of the receiver. The inversed RCS can be derived by subtracting the measured S_{21} of tag and sample ($S_{21}^{\mathrm{tag+sample}}$) with the measured S_{21} of metal sample without the tag (S_{21}^{sample}), instead of subtraction with $S_{21}^{\mathrm{background}}$. The inversed RCS can be expressed as

$$\mathrm{RCS'}_{\mathrm{tag+sample}} = \left[\frac{S_{21}^{\mathrm{tag+sample}} - S_{21}^{\mathrm{sample}}}{S_{21}^{\mathrm{ref}} - S_{21}^{\mathrm{background}}}\right]^2 \cdot \mathrm{RCS}_{\mathrm{ref}} \quad (3)$$

The $\mathrm{RCS'}_{\mathrm{tag+sample}}$ removes the reflection from metal sample in calculation only, therefore, it still contains the information of crack because the crack affects the absorptive resonant peak of the CMPA.

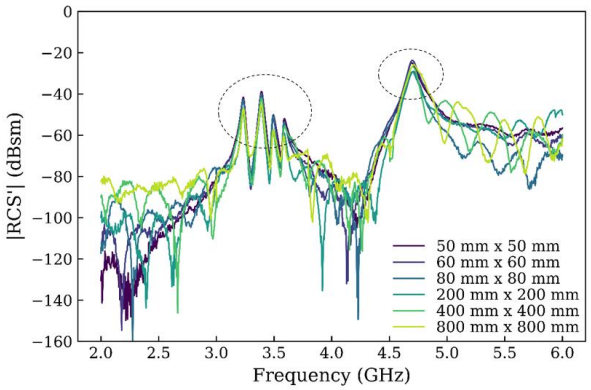

Fig. 15. Measured RCS' spectra using (3) of the chipless RFID sensor tag placed on different sizes of metal sample showing readable tag for any size of metal

A. Readability of the Chipless RFID Sensor Tag

Chipless RFID sensor tag readability is determined by the observability of the resonant frequencies representing the tag ID and the sensor's resonant frequency. The experimental investigation is started with the measurement of RCS spectrum when the chipless RFID sensor tag attached on a 60 mm x 60 mm metallic plate without crack. The reading distance is set at 30 cm as in the simulation. A comparison between the simulated and the measured RCS spectrum is presented in Fig. 12. As can be seen, the measured RCS agrees very well with the simulated one. Four resonant frequencies representing the tag ID of '1111' and a resonant frequency of CMPA at approximately 4.70 GHz can be observed in the RCS. It means that the chipless RFID sensor tag is definitely readable from 30 cm reading distance. Little discrepancies between the simulated and the measured RCS, especially the resonant frequencies, may be due to the fabrication error.

Next, the readability of the sensor tag is examined with longer reading distances. RCS spectra with reading distances of 30 cm, 60 cm, 90 cm, and 120 cm, are measured and the results are shown in Fig. 13. Data of $S_{21}^{\mathrm{tag+sample}}$, $S_{21}^{\mathrm{background}}$ and S_{21}^{ref} are acquired at every reading distance in the measurements. It is apparent that all resonant frequencies in the RCS are observable from any distance, which means that reading distance does not significantly affect the tag's readability in the anechoic chamber. Indeed, increasing the reading distance will add more ripples into the RCS. But, it is not a serious issue as long as magnitude of the ripples is small as compared to the resonant frequency notches.

In SHM applications, size of the monitored metallic structures is comparatively much larger than the samples used in this experiment. To examine the readability of the sensor tag, the RCS spectrum is measured at 30 cm reading distance over different sizes of metal. It is obvious from Fig. 14 that the larger metal surface will increase the overall RCS magnitude but will attenuate the resonant frequencies. When the size of

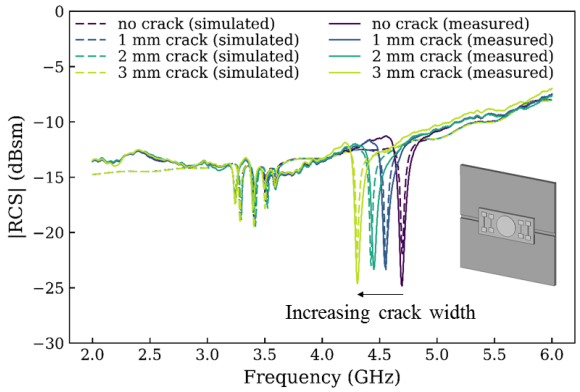

(a)

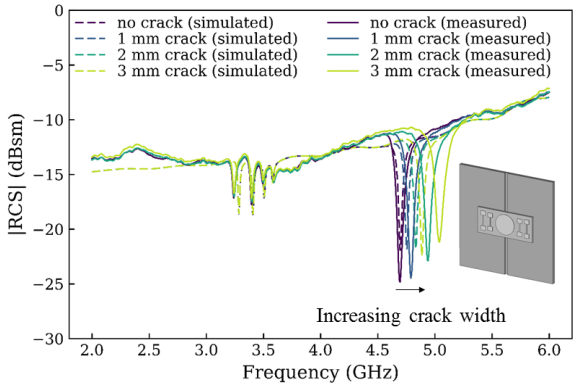

(b)

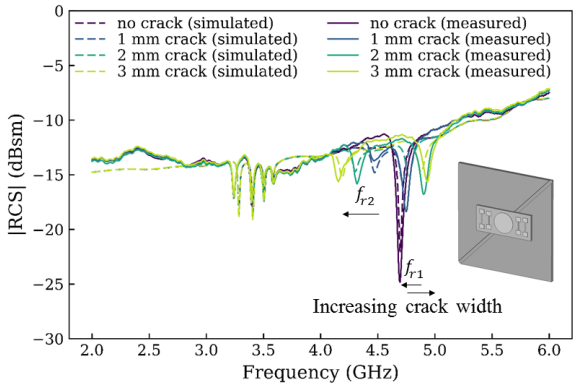

(c)

Fig. 16. Measured RCS spectra of the chipless RFID sensor tag validating the simulated results of resonant frequency shift for different crack orientations and widths: (a) Horizontal crack, (b) Vertical crack, (c) Diagonal crack

metal is 80 mm x 80 mm, the resonant frequencies are still observable. However, they are unobservable if the metal size is 200 mm x 200 mm. The reason is that the considerable amount of reflection from a large metallic surface tends to conceal the absorptive peaks of the resonators. Fortunately, as stated earlier, we can remove the reflection by applying the inversed RCS (RCS') as written in (3). The measured RCS' spectra for different sizes of metal are presented in Fig. 15. It is clear that the resonant frequencies are observable for all metal sizes by using RCS'. The resulting resonant frequencies from RCS' from (3) are definitely same as that from RCS based on (2). It is important to note that although the large metal can be calibrated using (3), the measurement becomes

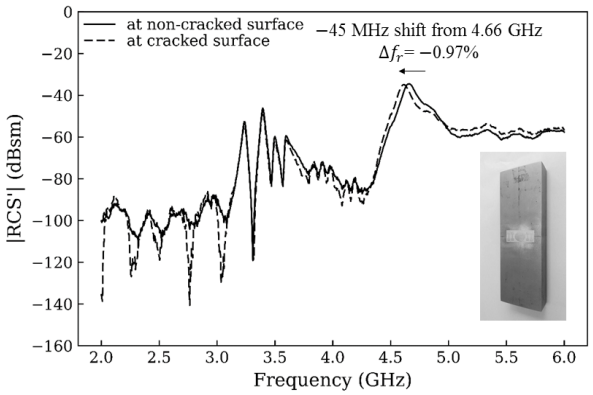

Fig. 17. Measured RCS' spectra showing detection of a microscopic natural fatigue crack by using resonant frequency shift

more sensitive to noise and any displacement of objects in the system. The large metal sample and the other metallic objects inside the chamber, e.g. reader antennas, produces a strong multipath that increases the noise level in the RCS'.

B. Experimental Study with Artificial and Natural Fatigue Cracks

The simulation results have shown that the direction (positive/negative sign) of resonant frequency shift corresponds to the crack orientation while its magnitude is proportional to the crack width. For validation, RCS measurements are performed with artificial crack samples. We measured the RCS spectrum of three crack widths, i.e. 1 mm, 2 mm, and 3 mm, for each crack orientation. The comparison between the simulated and the measured RCS spectra are given in Fig. 16. It is clear that, the simulated and measured results show a very good agreement in trend. In Fig. 16(a), measurement with horizontal crack samples shows that the resonant frequency is shifting towards lower frequencies as the crack width increased. The sign of the resonant frequency shift becomes negative and its magnitude represents the width of horizontal crack. The measured results with vertical crack samples in Fig. 16(b) also provide the same trend with the simulated results. The resonant frequency is shifting toward higher frequencies as the crack width increased. The sign of the resonant frequency shift is positive and its magnitude becomes higher when the vertical crack is wider. Additionally, the measured results of diagonal crack detection in Fig. 16(c) also demonstrate that the simulation results are valid.

Although the artificial cracks are sufficient for representing real cracks, testing the sensor tag with a natural fatigue crack is necessary to examine the detection reliability. Since the natural fatigue crack sample is considerably large in comparison with the sensor tag, we apply the RCS' as in (3) to observe the tag's resonant frequencies. The natural fatigue crack sample is placed upright at the sample holder so that the orientation of natural fatigue crack to detect is horizontal. The RCS' is measured with the tag attached at a non-cracked surface and at a cracked surface. The measured RCS' spectra at both locations on the metal surface are shown in Fig. 17. As can be seen, placing the sensor tag at the cracked surface shifts the resonant frequency as much as –45 MHz, or –0.97% from

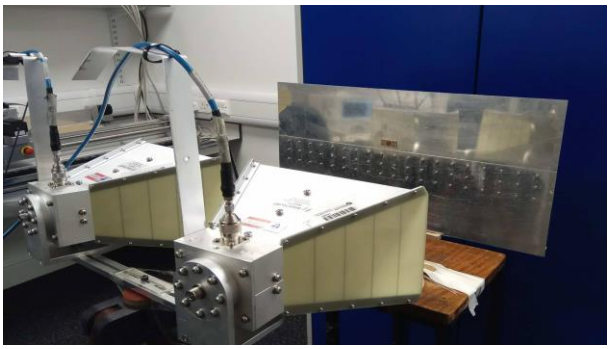

Fig. 18. Experiment setup outside the anechoic chamber

the original resonant frequency (4.66 GHz). By relying the detection sensitivity as –0.28% shift per 0.1 mm crack width obtained from simulation, the detection result of natural fatigue crack in the experiment does make sense. The resonant frequency shift of –0.97% implies that a horizontal natural fatigue crack with approximately 0.3 mm is detected.

C. Experimental Study outside the Anechoic Chamber

To examine the applicability of the chipless RFID sensor system in real environment, we perform an experimental study outside the anechoic chamber as depicted in Fig. 18. The experiment is conducted with some artificial crack samples mounted on a large metallic surface with size of 80 cm x 80 cm. The measurement setup is surrounded by various metallic objects such as a cabinet, computer, VNA, chairs tables, and so on. Distance

D. Limitations and Practical Challenges

Innovation in sensor tag design is one of the primary challenges in metal crack detection that should consider many aspects. The fundamental design aspects have been elaborated in Section III, so this subsection will partly discuss some other considerations for design improvement. In this study, the proposed sensor tag can detect a crack only when the crack is located behind the sensor resonator. It implies the metal areas behind the ID resonators are blind spots which should not exist or to be as small as possible. Still keeping the number of bit (the tag coding capacity) in mind, the ID resonators part should cover less surface area of the monitored metallic structure than the sensor resonator to minimize the blind spots. Additionally, the resonant frequencies representing the tag ID should be more observable by making the resonators more absorptive. For example, the resonant frequencies from dipole resonators in this work are less observable than that from CMPA. Hence, the tag ID might be difficult to read in certain conditions. The resonator design for ID part should be improved to have better resonating/absorption characteristics. One more design challenge is related to material and realization of the sensor tag. Chipless RFID sensor tag for metal crack detection has a potential to be fully printed on a flexible and adhesive substrate. The inkjet printing technique with silver/copper nanoparticle ink is commonly used for prototyping. In this case, the impacts of material and electrical properties of conductive ink to the crack detection performance need to be investigated. For industrial applications, the fully printable chipless RFID is a way to enable crack sensing skin which can be applied as metal coatings.

Despite of the sensor tag design, one practical challenge is associated with robustness of the sensor tag reading. A major drawback of the reading mechanism used in this work is it needs calibration measurements with the metallic structure without the attachment of tag as in (3). Nevertheless, performing subtraction with the monitored metallic structure makes the system very sensitive to positional change and any movement of the structure after calibration measurements done. Aside from the metal size problem, calibration measurements also requires the sensor system and the environment to be static and isolated. Consequently, the proposed chipless RFID sensor system is only reliable in an anechoic chamber environment. To be applied in real environment, the chipless RFID sensor system should be calibration-free [37] and robust in facing several factors: reflection of surrounding objects, the multipath, and the other changes/disturbances that makes the system not static. One potential solution is to use depolarizing sensor tags and the cross-polarization reading [38].

Regarding the crack detection performance, the proposed sensor tag has demonstrated its capability in characterizing crack width for horizontal, vertical, and diagonal orientation. The resonant frequency shift is found as a feature able to sensitively differentiate the crack width. The limitation is only with the detection of diagonal cracks when Δf_{r2} is unobservable. Therefore, enhancement of detection capability in classifying crack size, orientation, and location can be studied further. The challenge is to propose a better characterization or quantitative non-destructive evaluation (QNDE) method with feature extraction and selection as well as multiple feature fusion based on analysis of RCS magnitude or phase characteristics.

RFID array is a further practical challenge aiming at expanding the measurement space to localize metal cracks. In the implementation, a number of chipless RFID sensor tags having different ID is deployed as an array for area monitoring. Therefore, the chipless RFID sensor reader need to be embedded with an anti-collision algorithm [39] for reading multiple tags and separating sensor data according to the tag ID. Study on chipless RFID array is vital to discover how dense the sensor tags can be placed and read over a monitored metallic structure.

VI. Conclusion and Future Work

A novel use of the frequency signature based chipless RFID for metal crack detection and characterization has been demonstrated and validated by both simulation and experimental studies. We have provided a proof of concept by proposing a chipless RFID sensor tag design integrating dipole resonators as ID encoders and circular microstrip patch antenna (CMPA) resonator as a crack sensor. The sensor tag generates a frequency signature in the form of radar cross

section (RCS), showing multiple resonant frequencies, which represent the tag's ID and the sensor data. Resonant frequency shift of the CMPA is found as a feature able to indicate two crack parameters, i.e. crack orientation and crack width, on a metallic structure. Direction of resonant frequency shift can indicate the crack orientation while the magnitude of shift is proportional to the increase of crack width. A horizontal crack shifts the resonant frequency of CMPA toward lower frequencies, and oppositely, a vertical crack shifts the resonant frequency of CMPA toward higher frequencies. Meanwhile, a diagonal crack splits the resonant frequency into two where the shift of one of them has a linear relationship with the crack width. The detection sensitivity is remarkable. Several MHz to tens MHz resonant frequency shift is observable per 0.1 mm increase in crack width. Therefore, the proposed sensor tag has a capability to detect a submillimeter natural fatigue crack on a steel bar as expected. Furthermore, this work sets the reading distance at 30 cm, which can be extended. The chipless RFID sensor tag is still readable with a reading distance of 1.2 m.

According to the highlighted limitations and practical challenges with the proposed system, one of the crucial future works is to redesign the sensor tag and to implement a reader with signal processing capability so that the system is robust and applicable in real environment. Aside from the sensor tag design, feature extraction and selection method as well as signal processing techniques will play important roles. This issue is already being tackled by the authors.

REFERENCES

[1] J. P. Lynch, C. R. Farrar, and J. E. Michaels, "Structural health monitoring: Technological advances to practical implementations," *Proceedings of the IEEE*, vol. 104, no. 8, pp. 1508-1512, Aug. 2016.

[2] A. Zanella, N. Bui, A. Castellani, L. Vangelista, and M. Zorzi, "Internet of things for smart cities," *IEEE Internet Things J.*, vol. 1, no. 1, pp. 22-32, Feb. 2014.

[3] S. C. Li, L. D. Xu, and S. S. Zhao, "The internet of things: a survey," *Information Systems Frontiers*, vol. 17, no. 2, pp. 243-259, Apr. 2015.

[4] F. A. Iddings, "The basics of liquid penetrant testing," *MatEv*, vol. 44, no. 12, pp. 1364-1364, Nov. 1986.

[5] B. W. Drinkwater, and P. D. Wilcox, "Ultrasonic arrays for non-destructive evaluation: A review," *NDT&E Int.*, vol. 39, no. 7, pp. 525-541, Oct. 2006.

[6] J. Garcia-Martin, J. Gomez-Gil, and E. Vazquez-Sanchez, "Non-destructive techniques based on eddy current testing," *Sensors*, vol. 11, no. 3, pp. 2525-2565, Mar. 2011.

[7] V. P. Vavilov, and D. D. Burleigh, "Review of pulsed thermal NDT: Physical principles, theory and data processing," *NDT&E Int.*, vol. 73, pp. 28-52, Jul. 2015.

[8] M. U. Memon, and S. Lim, "Review of electromagnetic-based crack sensors for metallic materials (recent research and future perspectives)," *Metals*, vol. 6, no. 8, Aug. 2016.

[9] Y. Yao, S. T. E. Tung, and B. Glisic, "Crack detection and characterization techniques-An overview," *Structural Control & Health Monitoring*, vol. 21, no. 12, pp. 1387-1413, Dec. 2014.

[10] J. Zhang, G. Y. Tian, A. M. Marindra, A. I. Sunny, and A. B. Zhao, "A review of passive RFID tag antenna-based sensors and systems for structural health monitoring applications," *Sensors*, vol. 17, no. 2, Jan 29. 2017.

[11] Z. L. Zhaozong Meng, "RFID tag as a sensor - A review on the innovative designs and applications," *Measurement Science Review*, vol. 16, no. 6, pp. 305–315, Dec. 2016.

[12] S. Caizzone, and E. DiGiampaolo, "Wireless passive RFID crack width sensor for structural health monitoring," *IEEE Sensors J.*, vol. 15, no. 12, pp. 6767-6774, Dec. 2015.

[13] X. H. Yi, C. H. Cho, J. Cooper, Y. Wang, M. M. Tentzeris, and R. T. Leon, "Passive wireless antenna sensor for strain and crack sensing-electromagnetic modeling, simulation, and testing," *SmMaS*, vol. 22, no. 8, Aug. 2013.

[14] J. Zhang, G. Y. Tian, and A. B. Zhao, "Passive RFID sensor systems for crack detection & characterization," *NDT&E Int.*, vol. 86, pp. 89-99, 3//. 2017.

[15] S. Preradovic, and N. C. Karmakar, "Chipless RFID: Bar code of the future," *IEEE Microw. Mag.*, vol. 11, no. 7, pp. 87-97, Dec. 2010.

[16] S. Tedjini, N. Karmakar, E. Perret, A. Vena, R. Koswatta, and R. E-Azim, "Hold the chips," *IEEE Microw. Mag.*, vol. 14, no. 5, pp. 56-65, Jul-Aug. 2013.

[17] N. C. Karmaker, "Tag, you're it: radar cross section of chipless RFID tags," *IEEE Microw. Mag.*, vol. 17, no. 7, pp. 64-74. 2016.

[18] S. Preradovic, and N. Karmakar, "Chipless RFID tag with integrated sensor," in *Proc. IEEE Sensors*, 2010, pp. 1277-1281.

[19] A. Vena, L. Sydanheimo, M. M. Tentzeris, and L. Ukkonen, "A fully inkjet-printed wireless and chipless sensor for CO2 and temperature detection," *IEEE Sensors J.*, vol. 15, no. 1, pp. 89-99, Jan. 2015.

[20] E. M. Amin, N. C. Karmakar, and B. W. Jensen, "Fully printable chipless RFID multi-parameter sensor," *SeAcA*, vol. 248, pp. 223-232, Sep 1. 2016.

[21] S. Dey, P. Kalansuriya, and N. C. Karmakar, "Chipless RFID based high resolution crack sensing through SWB technology," in *Proc. IEEE Int. Microw. and RF Conf.*, 2014, pp. 330-333.

[22] S. D. Jang, B. W. Kang, and J. Kim, "Frequency selective surface based passive wireless sensor for structural health monitoring," *SmMaS*, vol. 22, no. 2, Feb. 2013.

[23] V. Palazzi, C. Mariotti, F. Alimenti, M. Virili, G. Orecchini, P. Mezzanotte, and L. Roselli, "Demonstration of a chipless harmonic tag working as crack sensor for electronic sealing applications," *Wireless Power Transfer*, vol. 2, no. 2, pp. 78-85, 2015/009/001. 2015.

[24] I. Mohammad, and H. Y. Huang, "An antenna sensor for crack detection and monitoring," *Adv. Struct. Eng.*, vol. 14, no. 1, pp. 47-53, Feb. 2011.

[25] F. Costa, S. Genovesi, and A. Monorchio, "A chipless RFID readable on metallic objects," in *Proc. IEEE Antennas and Propag. Soc. Int. Symp.*, 2013, pp. 1498-1499.

[26] F. Costa, S. Genovesi, and A. Monorchio, "Chipless RFIDs for metallic objects by using cross polarization encoding," *IEEE Trans. Antennas Propag.*, vol. 62, no. 8, pp. 4402-4407, Aug. 2014.

[27] I. Jalaly, and I. D. Robertson, "RF barcodes using multiple frequency bands," in *Proc. IEEE MTT-S Int. Microw. Symp.*, 2005, pp. 139-142.

[28] J. Machac, M. Polivka, M. Svanda, and J. Havlicek, "Reducing mutual coupling in chipless RFID tags composed of U-folded dipole scatterers," *MiOTL*, vol. 58, no. 11, pp. 2723-2725, Nov. 2016.

[29] C. M. Nijas, U. Deepak, P. V. Vinesh, R. Sujith, S. Mridula, K. Vasudevan, and P. Mohanan, "Low-cost multiple-bit encoded chipless RFID tag using stepped impedance resonator," *IEEE Trans. Antennas Propag.*, vol. 62, no. 9, pp. 4762-4770, Sep. 2014.

[30] F. Costa, S. Genovesi, and A. Monorchio, "A chipless RFID based on multiresonant high-impedance surfaces," *IEEE Trans. Microw. Theory Techn.*, vol. 61, no. 1, pp. 146-153, Jan. 2013.

[31] M. M. Khan, F. A. Tahir, M. F. Farooqui, A. Shamim, and H. M. Cheema, "3.56-bits/cm(2) compact inkjet printed and application specific chipless RFID tag," *IEEE Antennas Wireless Propag. Lett.*, vol. 15, pp. 1109-1112. 2016.

[32] P. Kalansuriya, N. C. Karmakar, and E. Viterbo, "On the detection of frequency-spectra-based chipless RFID using UWB impulsed interrogation," *IEEE Trans. Microw. Theory Techn.*, vol. 60, no. 12, pp. 4187-4197, Dec. 2012.

[33] A. Daliri, A. Galehdar, W. S. T. Rowe, K. Ghorbani, and S. John, "Utilising microstrip patch antenna strain sensors for structural health monitoring," *JIMSS*, vol. 23, no. 2, pp. 169-182, Jan. 2012.

[34] C. A. Balanis, *Antenna theory: analysis and design*: Wiley, 2015.

[35] X. Xu, and H. Huang, "Multiplexing passive wireless antenna sensors for multi-site crack detection and monitoring," *SmMaS*, vol. 21, no. 1, Jan. 2012.

[36] A. Vena, E. Perret, and S. Tedjini, "Design of compact and auto-compensated single-layer chipless RFID tag," *IEEE Trans. Microw. Theory Techn.*, vol. 60, no. 9, pp. 2913-2924, Sep. 2012.

[37] F. Costa, S. Genovesi, and A. Monorchio, "Normalization-Free Chipless RFIDs by Using Dual-Polarized Interrogation," *IEEE Trans. Microw. Theory Techn.*, vol. 64, no. 1, pp. 310-318, Jan. 2016.

[38] A. Vena, E. Perret, and S. Tedjni, "A depolarizing chipless RFID tag for robust detection and Its FCC compliant UWB reading system," *IEEE*

Trans. Microw. Theory Techn., vol. 61, no. 8, pp. 2982-2994, Aug. 2013.

[39] R. Rezaiesarlak, and M. Manteghi, "A space-time-frequency anticollision algorithm for identifying chipless RFID tags," *IEEE Trans. Antennas Propag.*, vol. 62, no. 3, pp. 1425-1432, Mar. 2014.

Adi Mahmud Jaya Marindra received a degree in Electrical Engineering from Gadjah Mada University, Indonesia, in 2010 and received a master's degree in Computer Engineering from King Mongkut's Institute of Technology Ladkrabang, Thailand, in 2013. After his graduation, he joined the RF Electronics research group at the National Electronics and Computer Technology Center (NECTEC) Thailand, where he worked on printed RFID. Since 2015, he has been a lecturer at Kalimantan Institute of Technology, Indonesia. He is currently working toward the PhD degree at the School of Electrical, Electronics and Computer Engineering, Newcastle University, UK. His main research interests are antennas and propagation, RFID, and wireless sensors.

Gui Yun Tian (M'01–SM'03) received the B.Sc. degree in metrology and instrumentation and M.Sc. degree in precision engineering from the University of Sichuan, Chengdu, China, in 1985 and 1988, respectively, and the Ph.D. degree from the University of Derby, Derby, U.K., in 1998. He was a Lecturer, a Senior Lecturer, a Reader, a Professor, and the Head of the Group of Systems Engineering, University of Huddersfield, Huddersfield, U.K., from 2000 to 2006. Since 2007, he has been with Newcastle University, Newcastle upon Tyne, U.K., where he is a Chair Professor of sensor technologies. Currently, he is also an Adjunct Professor with School of Automation Engineering, University of Electronic Science and Technology of China. He has coordinated several research projects with the Engineering and Physical Sciences Research Council, the Royal Academy of Engineering, and FP7. He has also collaborated with leading industrial companies such as Airbus, Toulouse, France, Rolls Royce, Derby, U.K., BP, London, U.K., nPower, Swindon, U.K., and TWI.